ALOS PALSAR quality assessment, calibration, and validation research

PI Number 175
Charles Werner[(1)]
Urs Wegmüller[(2)]

[(1)] Gamma Remote Sensing AG, Worbstrasse 225, CH-3073 Gümligen, Switzerland; E-mail: cw@gamma-rs.ch
[(2)] Gamma Remote Sensing AG, Worbstrasse 225, CH-3073 Gümligen, Switzerland; E-mail: wegmuller@gamma-rs.ch

Abstract
The main objectives of this ALOS calibration and validation research project (PI Number 175) are:

1. PALSAR data quality assessment
2. Adaptation of GAMMA software for PALSAR data processing
3. Radiometric and geometric calibration and validation
4. Validation of the feasibility of PALSAR repeat-pass interferometry for DEM generation and differential interferometric deformation monitoring

Keywords: ALOS, PALSAR, SAR processing, calibration, SAR interferometry, DEM generation, deformation monitoring.

1. INTRODUCTION

The main overall objectives of this ALOS calibration and validation research project (PI Number 175) were:

1. PALSAR data quality assessment
2. Adaptation of GAMMA software for PALSAR data processing
3. Radiometric and geometric calibration and validation
4. Validation of the feasibility of PALSAR repeat-pass interferometry for DEM generation and differential interferometric deformation monitoring

1.1. PALSAR data quality assessment

The first step in sensor calibration is to independently measure the performance of each element in the SAR data acquisition, and processing chain. This is followed by tests of the instrument and processing systems to assure that the end-to-end system is capable of producing image products that meet engineering specifications. Each element under test must have well-defined inputs, either simulated or experimentally derived. Outputs generated using these input data are compared with the expected output and system requirements.

The second aspect of data quality assurance (DQA) is termed "in-line" DQA and requires characterization of the raw data and metadata of each data acquisition. A set of tests and procedures performed to make sure that the raw data have adequate quality for processing and evaluation of the processed images to determine that they are focused and calibrated. The pre-processing tests included checking for missing lines, generation of raw data histograms, calculation of both range and azimuth spectra, and measurement of the Doppler centroid across the swath and along-track. The effective number of looks in the processed image is an indicator of image focus. Agreement between estimates of the image focus parameter derived both analytically and from the data is a good indication of proper processing. Visual and numerical inspection of images acquired over uniform distributed targets readily reveals uncompensated radiometric trends in range and azimuth.

1.2. Adaptation of GAMMA software for PALSAR data processing

The software adaptation included:

- Achievement of compatibility with PALSAR data
- Assessment of PALSAR raw data quality and quality of processing images
- Cross-comparison of GAMMA MSP processing results with NASDA processed data
- Adaptation of ISP, DIFF&GEO, and LAT to the input of MSP and NASDA processed PALSAR data (for the different product levels)

PALSAR data processed with the MSP were compared with NASDA processed SLC, PRI, and GEC products. This comparison included radiometric and geometric comparison as well as the calculation of an auto-interferogram of SLC processed by the MSP with the same SLC processed by NASDA.

1.3. Radiometric and geometric calibration and validation

SLC data processed with the GAMMA MSP are corrected for the range spreading loss, the antenna pattern, and pixel size normalization. For the absolute radiometric calibration

a calibration constant is required. We independently determined the MSP absolute calibration constant.

Geometric verification of PALSAR products was done over sites where we have a digital elevation model available. The data were processed and terrain corrected geocoded and the geocoding accuracy was validated, starting from Level 0 and Level 1 data.

1.4. Validation of the feasibility of PALSAR repeat-pass interferometry for DEM generation and differential interferometric deformation monitoring

PALSAR repeat-pass pairs were processed to validate the quality of the interferometric products. These products include correlation maps, interferometric phase, DEMs, and differential interferograms generated from 2 and 3 passes. Data over a site with existing and available DEM data available are preferred. The differential interferometry studies require multiple passes of data acquired with small baselines while data acquired to generate DEMs should have a moderate baseline. The high bandwidth mode of PALSAR permits taking additional looks to reduce interferometric phase noise. Our investigations encompass different terrain types.

The set of useful baselines for DEM generation is dependent on the terrain and incidence angle. Perpendicular baselines in the range of 400-1000 meters in the 14 MHz BW mode (FBD) and 400-2000 meters in the 28 MHz mode (FBS) are most useful.

Repeat pass data for differential interferometric studies benefits from having as small a baseline as possible to. Phase variation due to terrain related phase must be subtracted from the interferogram to reveal the deformation signature. Small baselines reduce the constraints on the DEM accuracy required for removal of the topographic phase.

The performance of high-bandwidth L-Band SAR for differential interferometry over a long term was also of interest. Various terrain classes have different characteristics due to seasonal variations in ground cover and precipitation. The expectation is that the L-Band PALSAR will perform significantly better than C-band systems in this application. We also assessed the validity of long-term observations for monitoring of slower geophysical phenomena.

1.5. Development and assessment of novel processing techniques

Considering the time since we submitted our first RA 175 proposal significant time elapsed. Considering this we added the objective to develop and assess novel processing techniques and applications.

We are considering the following novel techniques / applications:

- offset tracking techniques for mapping of faster motion
- FBS – FBD cross-mode interferometry
- persistent scatterer interferometry
- identification and investigation of ionospheric effects
- Improved RFI suppression
- PALSAR ScanSAR interferometry

In a first phase after the PALSAR launch we focused our research on

- PALSAR data quality assessment
- Adaptation of GAMMA software for PALSAR data processing
- Radiometric and geometric calibration and validation

Some results of this work are summarized below in section 2.1. Overall this work was completed until the mid-term reporting. The main conclusions were that the PALSAR data are of high quality and that our processing software was successfully adapted.

In a second phase we evaluated SAR interferometry. The PALSAR data were found to be well suited for SAR interferometry. Considering the acquisition plan with many FBS and FBD acquisitions we focused then on the development and evaluation of interferometric techniques to process pairs with one FBS and one FBD acquisition, i.e. acquisitions acquired using different chirp bandwidths. These results are reported in section 2.2. We are fully satisfied with the outcome that data of these two modes can be combined interferometrically. While normal interferometry worked without extra development FBS – FBD mode interferometry is already a part of work dedicated to the development and assessment of novel processing techniques.

After that we addressed time series analysis methods used for deformation mapping and monitoring. For a full persistent scatterer analysis (PSI) a significant number of scenes is typically required. To be able to work with somewhat smaller stacks and also to achieve a better spatial coverage we developed a methodology starting from a multi-reference stack. The unwrapped multi-reference stack phases are then used as input to an SVD step which permits deriving a (single reference) time series. This work is described in section 2.3.

2. METHODS, RESULTS, AND DISCUSSION

This section is the detailed description of the actual research implemented including methods, results and discussion.

2.1. PALSAR raw data characteristics and SAR processing

2.1.1. PALSAR raw data characteristics

For PALSAR fine-beam single-polarization mode (HH) acquisitions we found characteristics as shown in Table 1. The Doppler spectrum at the center of the swath, modulo the SAR pulse repetition frequency is shown in Figure 1. The Doppler ambiguity was resolved using a multi-look beat frequency (MLBF) algorithm. The Doppler centroid as a function of range was estimated by cross-correlation of adjacent lines and is shown in Figure 2. It is important to notice that such high Doppler Centroid values and significant range dependence of the Doppler Centroid was only observed during the initial phase. Later on zero-Doppler steering was applied very successfully, so that the Doppler Centroids determined were all close to zero.

Table 1 ALOS PALSAR Fine-Beam raw data characteristics.

Radar Center Frequency:	1270.000 MHz
Polarization	HH
Range Bandwidth	28.000 MHz
Chirp Duration	27 micro-sec.
Range Sample rate (IQ)	32.000 MHz
Number of range samples/echo	10304
Number of echoes	32421
Number of bits/sample	5
Pulse Repetition Frequency (PRF)	2159.827 Hz

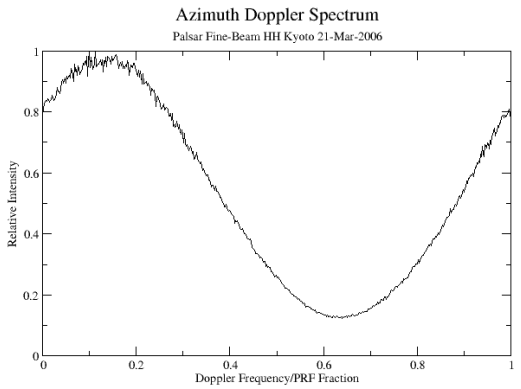

Figure 1. Azimuth spectrum at center-swath, modulo the SAR Pulse Repetition Frequency

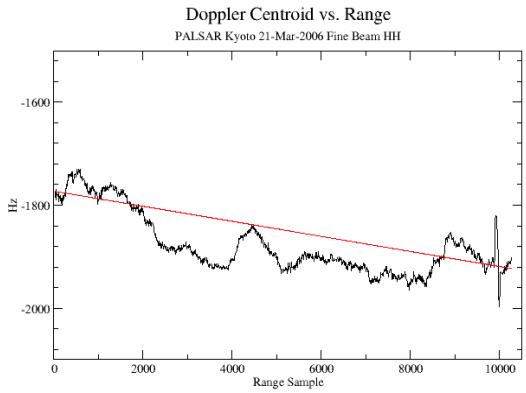

Figure 2. Doppler versus slant-range sample number (for a data set acquired early on before operation with zero Doppler steering).

2.1.2. SAR processing

Level-1 complex signal samples were processed using the Gamma MSP to produce single-look complex (SLC) and multi-look intensity (MLI) images. In fine-beam mode the transmit chirp is 28 MHz and lasts 27 micro-seconds.

The data were processed using a range-Doppler algorithm including secondary range migration. Autofocus confirmed that the effective along-track velocity determined from the state vectors was accurate at the level of .5 m/s. The antenna pattern provided are used for the radiometric calibration. A small section of a very early image processed with MSP showing the full range resolution and 3 azimuth looks is shown in Figure 3. Note the individual roads and buildings visible in the scene. For the 1 range x 3 azimuth looks MLI an equivalent number of looks (ENL) of 2.3 to 2.5 was determined. Radio-Frequency-Interference (RFI) filtering is applied.

Figure 3. Full range resolution section of the PALSAR Kyoto image acquired on 21-Mar-2006. The slant range sampling corresponds to an approx. ground range sampling of 7.9 m, the azimuth pixel spacing (3-look) is 9.55 m.

2.1.3. PALSAR Processing Point Target Response

In the processed SLC further analysis was performed to evaluate the point target performance in the image. A bright target was selected in the center of the image and analyzed using the Gamma point target analysis program to evaluate range and azimuth resolution, peak and integrated sidelobe levels and phase characteristic. Plots of range and azimuth cuts of the point target response are shown in Figures 4 and 5. Peak and integrated sidelobe levels are summarized in Table 2.

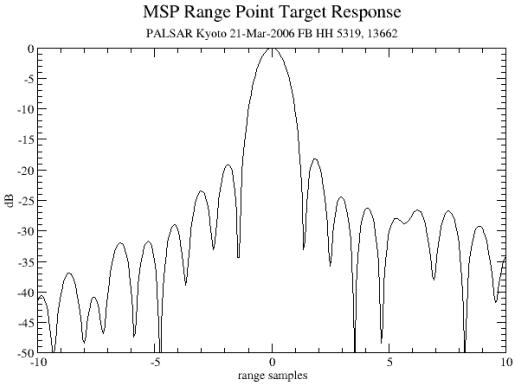

Figure 4. Point target response in range.

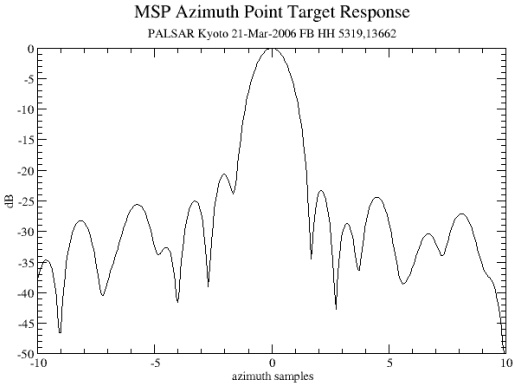

Figure 5. Point target response in azimuth.

Table 2. Point target resolution, peak side-lobe, and integrated side-lobe levels in range and azimuth.

range -3 dB width (samples):	1.188
range -10 dB width (samples):	1.996
range PSLR (dB):	-16.787
range ISLR (dB):	-16.851
azimuth -3 dB width (samples):	1.371
azimuth -10 dB width (samples):	2.332
azimuth PSLR (dB):	-20.661
azimuth ISLR (dB):	-18.247

2.2. FBS – FBD interferometry

2.2.1 FBS – FBD interferogram generation

In a first step each scene is processed individually using the appropriate chirp and sampling rates. Then a range over-sampling by a factor two is applied to the FBD scene to transform it to the same sample spacing as the FBS scene. Then the FBS SLC and the oversampled FBD scene are co-registered to a common reference geometry. Then we apply common band filter taking into account the smaller bandwidth of the FBD scene. And finally we calculate the interferogram.

Because of the high resolution sampling rate taking into account the terrain height in the resampling may be required. We do this by generation of a lookup table that relates the two SAR image geometries. This requires a DEM in the geometry of the reference scene image and precise state vectors. For each point in the reference scene we determine the location in the DEM that is being imaged. Then we determine at what time and slant-range that point is imaged by the radar in the second track. A refinement in the lookup table is performed using a cross-correlation analysis for small image patches. This approach resamples the SLC data at better than 1/10 pixel accuracy including baseline and terrain effects. Common-band filtering between the scenes can be done slope adaptively. The radar pulse samples a small bandwidth of the spatial reflectivity spectrum of the surface. For a particular frequency *f*, the equivalent wavenumber *k* at the surface is:

$$k_x = \frac{4\pi f}{c}\sin(\theta - \xi) \quad \theta: \text{look angle} \quad \xi: \text{surface slope}$$

The second interferometer antenna records a different part of the spectrum shifted by

$$\Delta f = \frac{f B_\perp}{2 r_0 \tan(\theta - \xi)} \quad B_\perp: Bperp \quad r_0: \text{SlantRange}$$

Spectral shift filtering removes the effect of baseline decorrelation for level surfaces. There is a proportional loss of range resolution.

2.2.2. Example

An example of a PALSAR FBS – FBD differential interferogram over a mining area in Poland is shown in Figure 5. The locations with excavation during the period considered can clearly be identified because of the dm scale subsidence occurring above the excavation. For further discussion of other examples it is referred to [1].

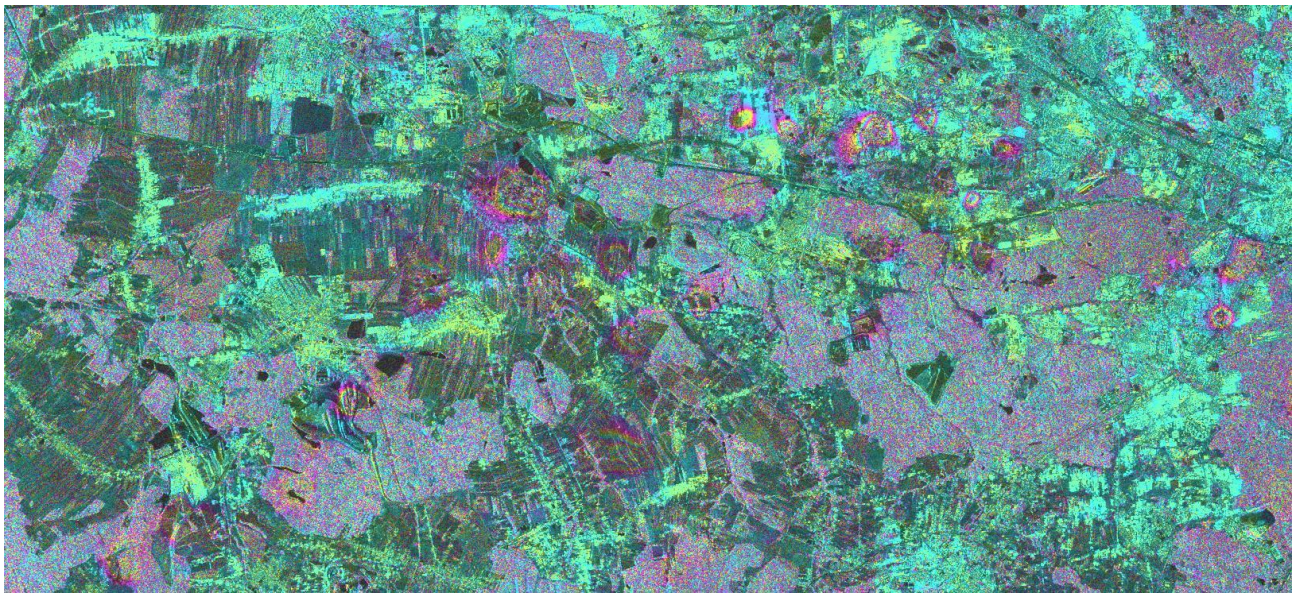

Figure 5. Section of a georeferenced PALSAR FBS – FBD differential interferogram over mining area in Poland, 20070222_20070710, Δt=138days, $B_{\perp}$=809m. One color cycle corresponds to 11.7cm displacement along the line-of-sight direction.

2.3. INSAR Time series analysis

2.3.1 Objective

Our objective was to use the a series of available PALSAR acquisitions to derive a complete deformation time series. At the time when we started this analysis we had 13 scenes available. For this purpose we developed a "hybrid INSAR" methodology using elements of conventional DINSAR, short baseline interferometry approaches, and PSI.

The data chosen was over of the Etna volcano. A strict uniform motion cannot be reasonably assumed and height dependent atmospheric path delays potentially affect the interferometric phase. Consequently, the developed methodology needs to address these aspects.

2.3.2 Methodology

The basic idea of the methodology developed was to derive the deformation time series from a set of differential interferograms with short time intervals and short baselines. The short temporal intervals are required to keep the level of deformation phase present low. For pairs with long intervals the deformation causes high phase gradients which may not be correctly resolved in the unwrapping. Using short spatial baselines optimizes the coherence and minimizes the topographic phase resulting from errors in the SRTM height reference which were used.

Table 2: Baselines and time intervals relative to the first scene

Nr	Pair	Bperp	dtime
1	20070127 20070127	0	0
2	20070127 20070614	1082	138
3	20070127 20070730	1608	184
4	20070127 20070914	1738	230
5	20070127 20071030	2303	276
6	20070127 20071215	2497	322
7	20070127 20080130	2888	368
8	20070127 20080316	3066	414
9	20070127 20080501	3733	460
10	20070127 20080616	-2877	506
11	20070127 20080916	-1341	598
12	20070127 20081101	-1017	644
13	20070127 20090201	-352	736

Table 3: Baselines and time intervals used for analysis

Nr	Pair	Bperp	dtime
0	20070127_20070614	1085	138
1	20070127_20080916	-1343	598
2	20070127_20081101	-1019	644
3	20070127_20090201	-353	736
4	20070614_20070730	525	46
5	20070614_20070914	656	92
6	20070614_20090201	-1438	598
7	20070730_20070914	130	46
8	20070730_20071030	696	92
9	20070914_20071030	565	46
10	20070914_20071215	760	92
11	20071030_20071215	194	46
12	20071030_20080130	586	92
13	20071215_20080130	391	46
14	20071215_20080316	569	92
15	20080130_20080316	178	46
16	20080130_20080501	847	92
17	20080316_20080501	669	46
18	20080616_20080916	1539	92
19	20080916_20081101	323	46
20	20080916_20090201	990	138
21	20081101_20090201	666	92

The baselines relative to the first scene are shown in Table 2. Pairs with short time intervals and short baselines nicely form a set well suited for the derivation of a time series with the exception of the interval between 1-May-2008 and 15-Jun-2008 which has a 6.6km baseline because an adjustment of the orbit. To also cover this time interval we included several pairs with a long time interval and a short spatial baseline. These pairs are important to connect the acquisitions before and after this orbit adjustment. The set of pairs used is listed in Table 3.

For all the selected pairs differential interferometric processing was done to derive unwrapped "deformation phases" using the following steps:

- raw data processing with range extension
- range oversampling of FBD scene to FBS sampling
- co-registration of SLCs to common geometry
- 2-pass differential interferometry using oversampled SRTM as initial height reference, updating of height reference based on very long baseline pair with short time interval (20080501_20080616), slope adaptive common band filtering, baseline refinement
- estimation and subtraction of a topography related atmospheric phase term
- phase unwrapping

The height dependent atmospheric phase effect was estimated over the mountains to the north of Etna and not over the Etna itself to avoid confusion between volcanic deformation and atmospheric phase.

Then, starting from the multi-reference stack of unwrapped phases we derived a single reference time series using Singular Value Decomposition (SVD) to obtain the least-squares solution for the phase time-series. A complete series is obtained for the times connected by the multi-reference pairs. Based on the 21 pairs we obtained the time series for the 13 acquisition dates. Redundancy in the differential interferogram input data reduces uncorrelated errors in the time-series. Uncorrelated errors include residual topographic phase errors and phase noise. Atmospheric phase on the other hand is not reduced by this estimation procedure. For a given acquisition date there is a well defined atmospheric phase delay pattern which is present in all the pairs including this date. The same applies for non-uniform deformation phase. Consequently, the obtained time series of unwrapped phases still includes the atmospheric phases as well as non-uniform deformation phase.

Apart from the phase time series the RMS deviation of the values from the SVD is calculated as a quality value, permitting to identify unwrapping errors which remained undetected.

Applying linear regressions to the time series we also estimated the linear deformation rates (Figure 6). Atmospheric phases as well as phases relating to non-uniform motion are part of the deviation of the time series from the linear regression. Temporal filtering was used, to separate temporally correlated (non-uniform deformation) and uncorrelated (atmospheric delay and phase noise) components.

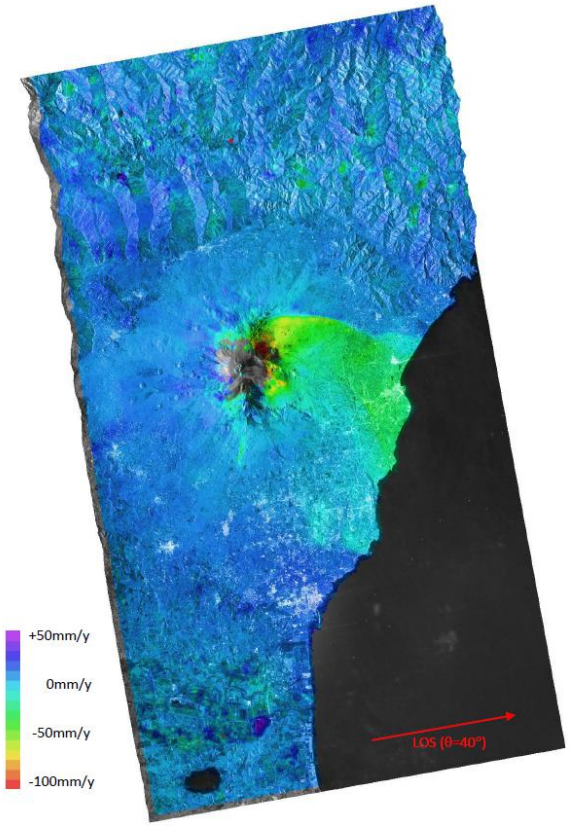

Figure 6 Average deformation rate (LOS component) determined from ALOS PALSAR data between 27-Jan-2007 and 1-Feb-2009 over the Etna Volcano

3. CONCLUSIONS

Overall our project was a success. Data access was good and timely and we could adapt our processing techniques and software successfully.

In the time series analysis some extra development was achieved to be able to get to good deformation time series for stacks of 10 to 20 images. Now we will also have stacks of > 20 scenes available to test more standard PSI processing.

We also acquired several PALSAR ScanSAR scenes to develop ScanSAR interferometry processing capability.

We attended all the ALOS PI Symposiums and presented our results. The timely adaptation of our processing software for PALSAR data was of great support for a large number of GAMMA software users in Japan and world-wide.

4. ACKNOWLEDGMENTS

ALOS PALSAR data were provided in the frame of JAXA's RA Program Project 175 "ALOS PALSAR quality assessment, calibration, and validation research".

5. PUBLICATIONS

[1] Wegmüller U., T. Strozzi, C. Werner, A. Wiesmann, V. Spreckels, N. Benecke, and D. Walter, "Monitoring of mining induced surface deformation", Procs First joint PI Symposium of ALOS data nodes for ALOS Science Program, 19-23. Nov. 2007, Kyoto, Japan.

[2] Werner C., U. Wegmüller, T. Strozzi, A. Wiesmann, and M. Santoro, "PALSAR Multi-Mode Interferometric Processing", Procs First joint PI Symposium of ALOS data nodes for ALOS Science Program, 19-23. Nov. 2007, Kyoto, Japan.

[3] Wegmüller U., C. Werner, and M. Santoro, Motion monitoring for Etna using ALOS PALSAR time series, ALOS PI Symposium 2009, 9-13 Nov. 2009 Hawaii, USA.

[4] Wegmüller U., Charles Werner, Maurizio Santoro, Pierre Briole, ALOS PALSAR deformation monitoring over Etna, Italy, ALOS PI Symposium 2010, 15-17 Nov 2010, Tokyo, Japan